



HAL
open science

Permafrost controls the displacement rates of large unstable rock-slopes in subarctic environments

I.M. Penna, Florence Magnin, P. Nicolet, B. Etzelmüller, R.L. Hermanns, M. Böhme, L. Kristensen, F. Noël, M. Bredal, J.F. Dehls

► **To cite this version:**

I.M. Penna, Florence Magnin, P. Nicolet, B. Etzelmüller, R.L. Hermanns, et al.. Permafrost controls the displacement rates of large unstable rock-slopes in subarctic environments. *Global and Planetary Change*, 2023, 220, pp.104017. 10.1016/j.gloplacha.2022.104017 . hal-03942667

HAL Id: hal-03942667

<https://hal.science/hal-03942667v1>

Submitted on 24 Nov 2023

HAL is a multi-disciplinary open access archive for the deposit and dissemination of scientific research documents, whether they are published or not. The documents may come from teaching and research institutions in France or abroad, or from public or private research centers.

L'archive ouverte pluridisciplinaire **HAL**, est destinée au dépôt et à la diffusion de documents scientifiques de niveau recherche, publiés ou non, émanant des établissements d'enseignement et de recherche français ou étrangers, des laboratoires publics ou privés.

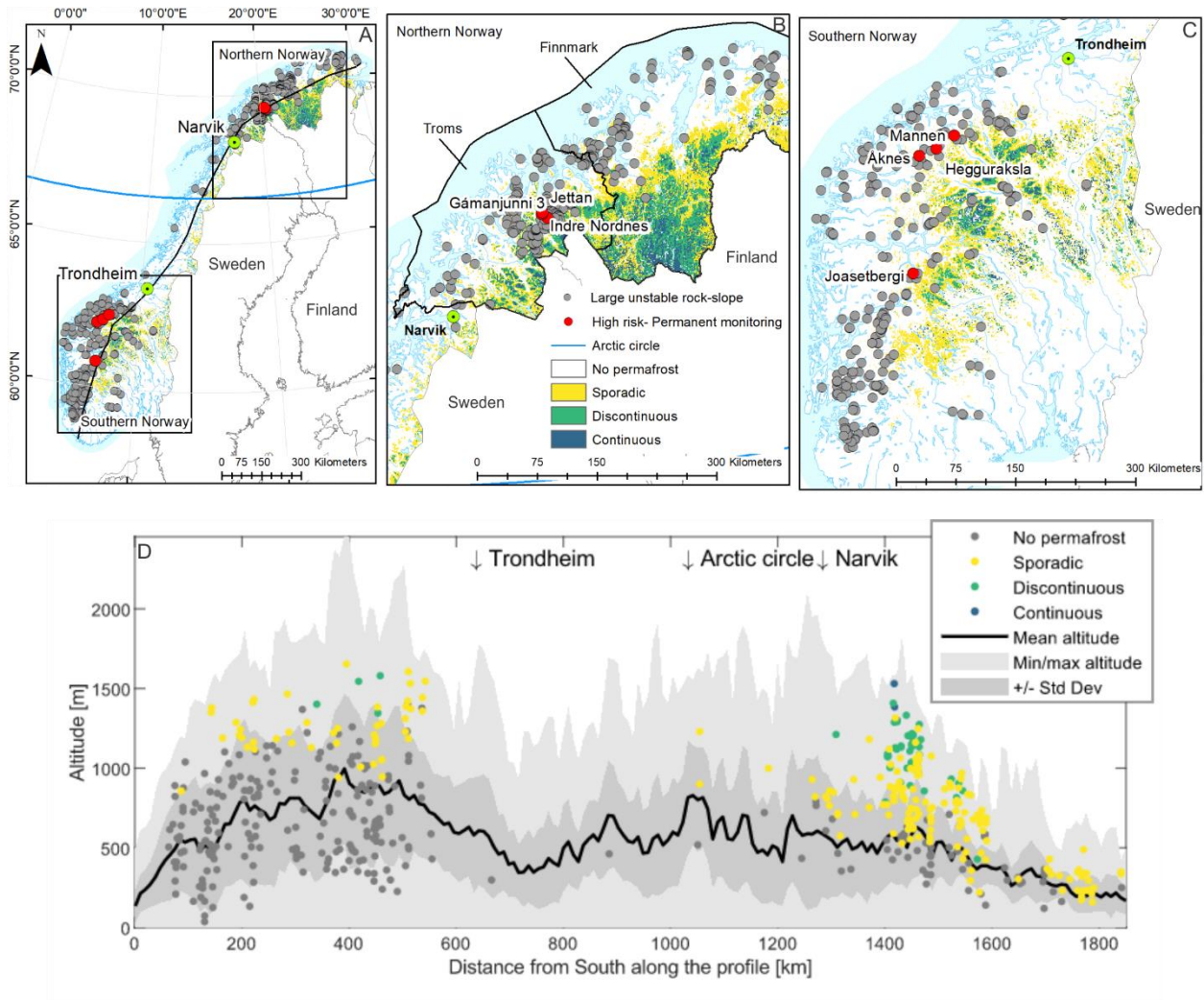
23 **Key words:** Subarctic; Permafrost thawing; Unstable rock-slopes; Displacement rates.

24 **1. INTRODUCTION**

25 Currently, permafrost underlays ca. 17 % of the Earth's land surface and ca. 15 % of the land surface
26 area in the Northern Hemisphere (Obu et al., 2019). Throughout the Holocene, its extent has fluctuated
27 significantly, from a minimum areal distribution at the Holocene Thermal Maximum to a maximum
28 expansion during the Little Ice Age (LIA) (Kondratjeva et al., 1993; Lilleøren et al., 2012). Its current
29 warming and thawing at a global scale (Biskaborn et al., 2019) has a number of environmental impacts
30 both globally – such as the release of greenhouse gasses –and locally – for example, in alpine and high-
31 latitude settings by affecting the stability of slopes (Haeberli et al., 1997; Gruber et al., 2004; Lewkowicz
32 and Harris, 2005; Huggel et al., 2012; Swindles et al., 2015; Liljedahl et al., 2016; Hjort et al., 2018;
33 Lewkowicz and Way, 2019).

34 In the last two decades, permafrost degradation has been found responsible for the occurrence of rock-
35 slope collapses in the Alps, with volumes ranging from thousands to hundreds of thousands of cubic
36 meters (Gruber et al., 2004, Allen et al., 2009, Ravanel et al., 2011, Ravanel et al., 2017). For failures of
37 that scale, the relation between the collapse and the degradation of the permafrost has been
38 established at a regional scale. However, for large rock-slope collapses, with volumes of several
39 hundreds of thousands or millions of cubic meters of rocks, any causal relationships that have been
40 proposed up to date are based upon a single or a small number of event investigations (Haeberli et al.,
41 1997; Fischer et al., 2010; Phillips et al., 2017; Svennevig et al., 2020; Shugar et al., 2021), theoretically
42 proposed in mechanical models and evaluated in laboratory experiments (Krautblatter et al., 2013), or
43 have been modelled with a numerical stability model, reproducing the mechanical response of rock-
44 slopes to permafrost degradation (Mamot et al., 2018). A step forward in the global understanding of
45 permafrost degradation as the first control of rock-slope deformation was made in a recent work

46 combining thermal ground conditions with paleo-slip rates of six unstable rock-slopes (Hilger et al.,
47 2021). This work postulated that the frequency of slope failures could increase under warming
48 conditions. But is the relationship so straightforward? Answering this question has implications for
49 understanding landscape evolution and geohazard scenarios and establishing appropriate development
50 strategies in high-mountain settings and arctic and subarctic regions. Norway, with more than 500 LURs
51 identified through a vast program for systematically mapping large unstable rock-slopes (LURs; fig. 1;
52 Blikra et al., 2006; Hermanns et al., 2013), and with current and past permafrost conditions covering
53 large part of its territory (Lilleøren et al., 2012; Gislås et al., 2016a; Magnin et al., 2019), is a perfect
54 natural laboratory to build into this knowledge. Our study statistically explores the link between
55 permafrost and displacement rates of LURs, by combining ground surface deformation rates
56 determined from satellite remote sensing for all of Norway (Dehls et al., 2019) and in-situ
57 measurements, with modelled current and past ground thermal conditions (Magnin et al., 2019; Gislås
58 et al., 2016b). Furthermore, the study expands the debate on how landslide hazards in current
59 permafrost areas might change with warmer climate conditions.



60

61 Figure 1. Observation of LURs and distribution of permafrost on the mainland of Norway. A) Location of

62 LURs and type of permafrost (combined from Gislås et al., 2016a and Magnin et al., 2019). The black

63 lines correspond to the profile displayed in figure D and. B) Location of LURs and type of permafrost in

64 northern Norway (NN) with indication of extension of Troms and Finnmark counties. C) Location of

65 LURs and type of permafrost in southern Norway (SN). D) Topographic profile from south to north with

66 locations of the headscarp of the LURs, classified by class of permafrost.

67

68

69 2. METHODOLOGY

70 2.1. Characterisation of large unstable rock-slopes

71 In this work we analyse 509 LURs with volumes larger than 100 000 m³ identified and mapped by the
72 Geological Survey of Norway (NGU) through a national systematic mapping and monitoring programme,
73 which started in 2007 (fig. 1; Oppikofer et al., 2015). Their identification was conducted by using high-
74 resolution (1-m or better) aerial photos and digital terrain models (DTM) and the use of a full national
75 satellite-based ground motion service (insar.ngu.no). The assessment of LURs carried out by NGU
76 includes field mapping, structural and kinematic analyses, monitoring of displacement rates, and in
77 some cases, the dating of sliding surfaces.

78 In this work we computed the average orientation of each LUR using the 10m DTM of Norway and the
79 perimeter of the LURs. We derived from the DTM the aspect (geodesic method) and slope in ArcMap
80 and used these inputs to calculate the normal vector in each cell of the DEM. We computed then a
81 weighted sum of all the normal vectors inside each LUR's polygon. We used the inverse of the cosine of
82 the slope to weight the sum since sloping cells of a DTM represent a larger surface area. Finally, the
83 aspect and slope of the surface represented by the resulting normal vector was computed.

84 Once the orientation was calculated for each LUR individually, we calculated the average orientation of
85 all the LURs in a region. To achieve this, we derived a horizontal unit vector from the aspect of each
86 LUR calculated previously and then sum all those vectors. If the LURs are all oriented in the same
87 direction, the resulting vector will be long, while if they are randomly distributed, this vector will be
88 short. To measure this, we compute the strength of the resulting vector (or mean resultant length),
89 which is defined as its length divided by the number of vectors summed (Borradaile et al., 2003). Thus, a
90 value of 1 means that all the vectors have the same orientation, while a value close to 0 reflects the
91 absence of preferential orientation.

92 We calculated the LURSS' volumes using the sloping local base-level (SLBL) method (Jaboyedoff et al.,
93 2020), which is an iterative method considering that the volume above a sloping surface connecting the
94 surrounding points, in that case the limits of the instability, can be eroded. A tolerance can be used to
95 create a curved surface, and the value of the tolerance controls the curvature. We implemented this
96 method in an ArcGIS toolbox (<https://github.com/ngu/pySLBL>). The developed tool calculates the
97 tolerance automatically for each LURS by drawing a profile going through the centre of the LURS's
98 polygon and following the average slope direction. The horizontal length (l) of the LURS and its altitude
99 difference (Δz) along this profile are used to estimate the tolerance (c) using the following formula:

$$100 \quad c = 2 \cdot (1 - \sqrt{2}) \cdot \Delta z \cdot \left(\frac{x^2}{l^2} \right)$$

101 where x is the cell size of the DTM. This formula gives a tolerance that is half of the maximum tolerance
102 defined in Oppikofer et al., 2016. From our experience, the tolerance as calculated in this study can be
103 considered acceptable. The volume is given by the difference between the original DTM and the
104 resulting DTM after applying the SLBL method, which represents the thickness of the LURS. The sum of
105 all the pixels of the raster of thickness, multiplied by the area of a pixel results in the volume of the
106 LURS.

107 **2.2. Measurement of displacement rates**

108 Displacement rates of 296 out of 509 LURSSs have been used in this work. Displacement rates were
109 extracted from the NGU database and own measurements using InSAR Norge portal. We use the
110 displacement rates that are representative of the whole LURSSs, not of single scenarios. Within the
111 framework of the hazard classification system done by NGU (Hermanns et al., 2012), six classes of
112 displacement have been defined: 1. No movement; 2. <0.5 cm/y; 3. 0.5-1 cm/y; 4. 1-4 cm/y; 5. 4-10

113 cm/y; and 6. >10 cm/y. LURs with unknown displacement rates are located mainly on slopes with dense
114 vegetation coverage, are in shadow zones of the Sentinel-1 satellites or are on inaccessible slopes.

115 The methods used for the monitoring of displacement rates are as follows:

116 Differential Global Navigation Satellite System (dGNSS): used to measure displacement rates on 95
117 LURs. The time the LURs have been monitored is variable, the longest monitored period with this
118 method spans from 2003 to 2018, and the time interval between the measurements depends on the
119 degree of activity each LURs, accessibility, estimated risk, among other factors. The measurements rely
120 on the installation of a network of one or several fixed points in stable outcrops and several points on
121 the unstable rock-mass. GNSS antennas are mounted for each acquisition campaign on bolts fixed to the
122 rocks. Static phase measurements are performed with an interval of a minimum of one year between
123 acquisitions. The measurements are then post-processed using the fixed point(s) as reference. The
124 displacement rate of the LURs is considered significant if both the following conditions are met:

- 125 • the displacement rate obtained by linear regression (v) is higher than the average measurement
126 accuracy (σ_{tot}) multiplied by the square root of two and divided by the time interval between
127 the first and the last measurement (Δt) in years:

$$128 \quad v > \frac{\sqrt{2} \cdot \sigma_{tot}}{\Delta t}$$

- 129 • the displacement follows a coherent trend over at least three measurements.

130 Tape extensometers: used on 34 LURs. Here, eye bolts are mounted on both sides of a structure (scarp,
131 crack, etc.), permitting the installation of the instrument at the same location for each acquisition.

132 Repeated measurements are performed with an interval of at least a year. The displacement rates are
133 given by the change of the length of the tape over the years. As for the GPS, a coherent trend shown by
134 at least three measurements (i.e. at least 2 years between the first and last measurement) is necessary
135 to consider the measured velocity reliable.

136 Interferometric Synthetic Aperture Radar (InSAR): compares microwave images acquired at different
137 times, allowing the detection of surface displacement rates down to mm/y scale, by analysing changes
138 in the phase of the returned microwave (Massonnet et al., 1998). The monitoring can involve both
139 satellite-based InSAR and ground-based InSAR (GB-InSAR) (Wasowski et al., 2014, Bertolo, 2017,
140 Kristensen et al., 2021).

141 Satellite InSAR measurements are based on Sentinel-1 images acquired since 2015 (freely available at
142 <https://insar.ngu.no>) and processed with the persistent scatterers method (Ferretti et al., 2000; Ferretti
143 et al., 2001). Sentinel-1 has a spatial resolution of 5 by 20 m, a swath width of 250 km, and a revisit
144 period of either 6 or 12 days between acquisitions. The measurements are one-dimensional along the
145 radar line-of-sight (LOS) and depend on the acquisition geometry. Thus, the accuracy of the method
146 depends on the angle formed by the LOS of the sensor and the vector of displacement of the LURS.

147 The LOS of the satellites is inclined either towards the west or the east. Therefore, LURs with stronger
148 northward or southward displacement will have their rates underestimated, but the vertical component
149 will be measured anyhow. The larger the angle between the displacement vector of a LURS and the LOS
150 of the satellite, the more we underestimate the real displacement of a LURS. However, since we are
151 mostly interested in the magnitude of the displacement the measurements (divided in classes) are
152 acceptable approximations of real displacement rates, but there is a risk of classifying some LURS in a
153 lower class of displacement. Because snow coverage hinders the measurements in winter, 2 m-high
154 corner reflectors have been installed on 23 LURs to allow for measurements throughout the year.

155 *Ground-Based InSAR* has been used on 9 LURs by the Norwegian Water Resources and Energy
156 Directorate (NVE). The measurements were computed along the LOS of a radar mounted to the ground,
157 typically in front of and below the LURS. This makes the instrument to have its LOS as parallel as possible
158 to the expected displacement vector. The LiSALab radar system, that measures in the Ku band, with a

159 central frequency of 17.2 GHz is used. The instruments can measure movements exceeding 1 m/day, but
160 since for some LURs the displacements range from a few mm to a few cm per year, periodic campaigns
161 (about a week in length) are conducted two or more times in a season or over a few years. These
162 campaigns are averaged to a single radar image, and the change of distance between the campaigns is
163 calculated. If a LUR has a very fast displacement, its rate is measured on a daily basis.

164 **2.3. Steep slopes permafrost mapping**

165 To assess current permafrost conditions on LURs, we extracted the minimum mean annual rock-surface
166 temperature (MARST) value inside the polygon representing each LUR and the corresponding
167 permafrost class (sporadic, discontinuous, continuous) from the 10 m resolution CryoWALL map from
168 Magnin et al. (2019), covering all slopes $> 40^\circ$ in a 10 m resolution DEM (fig. S6). When more than a class
169 of permafrost is present, we assign the one covering the largest area. For LURs in gentler slopes, we
170 assigned the class of permafrost using the regional permafrost model and MAGT temperatures from
171 Gislås et al. (2016b).

172 The MARST map derives from a multiple linear regression model, with mean annual air temperature
173 (MAAT) and potential incoming solar radiation (PISR) as explanatory variables. Magnin et al. (2019)
174 calibrated it with in-situ measurements (85 MARST measurement points), local MAAT records and
175 computed PISR at each measurement point using GIS tools. The predicted MARSTs and their standard
176 deviation were used to calculate a permafrost probability (probability that MARST is $\leq 0^\circ\text{C}$), and later
177 converted into a map of permafrost classes, with sporadic permafrost designating areas with permafrost
178 probability of 10 to 50%, discontinuous permafrost designating areas with probability ranging from 50 to
179 90% and continuous permafrost referring to areas with a probability of $>90\%$ (Magnin et al., 2019). Thus,
180 “sporadic permafrost” indicates conditions where permafrost may be very patchy and subsists because
181 of transient effects from past colder climates or because of locally favourable conditions (such as
182 fractured outcrops with air ventilation); “discontinuous permafrost” indicates more wide-spread areas,

183 but with permafrost temperatures closer to 0°C, while “continuous permafrost” indicates conditions
184 favourable to permafrost persistence independent of ground characteristics (fractured or not) or
185 debris/snow cover. A probability of 50 % corresponds to a MARST of 0°C.

186 For this study, we produced MARST and permafrost class maps for the Little Ice Age (LIA; ca. 250 y BP)
187 using the air temperature coefficient of the multiple linear regression model (1.06) and the LIA known
188 air temperature anomaly (compared to the 1961-1990 period). For the LIA anomalies, we used the value
189 -1.5°C, which is considered to be reasonable value based on various studies in the wider North-Atlantic
190 region (e.g. Lilleøren et al., 2012; Etzelmüller et al., 2020). As a first step, the air temperature difference
191 was calculated from the periods 1981-1990 and 1961-1990 from the SeNorge air temperature maps and
192 applied to the CryoWALL map (Magnin et al., 2019). Then, we considered the LIA for back analysis and
193 its respective air temperature anomaly of -1.5°C. For the LIA period, specific MARST, permafrost
194 probability and permafrost class maps were created and used to determine permafrost conditions on
195 LURs on steep slopes. For LURs of gentler slopes, the presence of permafrost during LIA was evaluated
196 using the map of Lilleøren et al. (2012) who modelled the distribution of Holocene permafrost in
197 Norway. Figure S1 shows an example of the MARST map and permafrost maps for the LIA and current
198 times (CT) for a LUR from northern Norway.

199 **2.4. Statistical analyses**

200 We performed statistical analyses to investigate the relation of different variables, namely permafrost,
201 minimum temperature, slope, area and lithology with the displacement rates of LURs. Other aspects
202 such as the structural control or the glaciation history were not considered as they are difficult to
203 investigate at that scale. To further identify if the considered variables are spatially related, the analyses
204 were done for the entire country, the South, the North, and two specific regions of the North: Troms
205 and Finnmark. Thus, the groups are not independent since Troms and Finnmark are included in the

206 North, which, together with the South, are included in the entire country. Because of the different
 207 nature of the studied variables (Table 1), various tests were performed.

208

209 Table 1. Tested variables and corresponding data types.

Variable	Type
LIA-CT permafrost	Categorical ordinal
CT permafrost	Categorical ordinal
Min MARST	Interval
Displacement rate	Categorical ordinal
Area	Ratio
Rock type	Categorical nominal
Slope	Ratio

210 Note: The LIA-CT permafrost is a combination of two ordinal scales. It allows calculating Kendall's τ .

211 Displacement rate is considered on a categorical scale since the available displacement data does not
 212 always allow accurate measurement of the displacement rate. Here we sort the classes primarily by CT
 213 and secondarily by LIA to use the combination scale as an ordinal scale.

214 The Chi-squared method (Pearson et al., 1900) is applied here when both variables are categorical. The
 215 observed Chi-squared is given by:

216
$$X^2 = \sum_{i=1}^n \frac{(O_i - E_i)^2}{E_i} \quad (\text{eq. 1})$$

217 where O_i is the observed number of events in class i and E_i is the expected number of events in the
 218 same class assuming no correlation (null hypothesis). The p-value is then calculated from the Chi-
 219 squared distribution using the corresponding degrees of freedom, calculated as follows:

220 $dof = (m - 1) * (n - 1)$ (eq. 2)

221 where m and n are the number of classes for the two parameters, respectively. The p-value gives the
222 probability for the Chi-squared, assuming the null hypothesis, to be higher than the observed Chi-
223 squared. Thus, the lower the p-value, the less likely the data is to fulfil the null hypothesis. It is
224 commonly considered that the null hypothesis is rejected for p-values below 0.05 (Borradaile, 2003),
225 which implies that the alternative hypothesis (i.e., that the variables are correlated) is then accepted.
226 Here, we considered the correlation to be significant for p-values below 0.01, partly significant for p-
227 value between 0.01 and 0.1 and not significant for p-values above 0.1. It is recommended to apply the
228 Chi-squared method only when the expected number of events is at least 5 for each class (Borradaile et
229 al., 2003). Here we classify the velocities in fewer classes (no movement, significant movement <1cm/y,
230 >1cm/y) to avoid having classes with too few values, and only use the classes of the other parameters
231 (rock type or permafrost type) when there are at least ten values in them. Even when using fewer
232 classes, we do not always reach the minimum expected value of 5 events in each class, so we present
233 the minimum expected value as a control so that the analyses where this threshold is not reached can
234 be interpreted more carefully (Table S1).

235 Kendall's τ calculates the association between two rankings. It is calculated from the following equation:

236
$$\tau = \frac{C - D}{\sqrt{\left(\frac{n(n-1)}{2} - T_x\right)\left(\frac{n(n-1)}{2} - T_y\right)}} \quad (\text{eq. 3})$$

237 where C is the number of concordant pairs, D the number of discordant pairs, n the number of data
238 points, T_x the number of ties on x and T_y the number of ties on y (Agresti, 2010). A concordant pair is a
239 pair (x_1, y_1) and (x_2, y_2) where either $x_1 > x_2$ and $y_1 > y_2$ or $x_1 < x_2$ and $y_1 < y_2$. Kendall's τ takes a
240 value between -1 and 1, where -1 indicates a perfect monotonically decreasing relation, 1 indicates a
241 perfect monotonically increasing relation and 0 indicates the absence of relation. Again, we calculated a

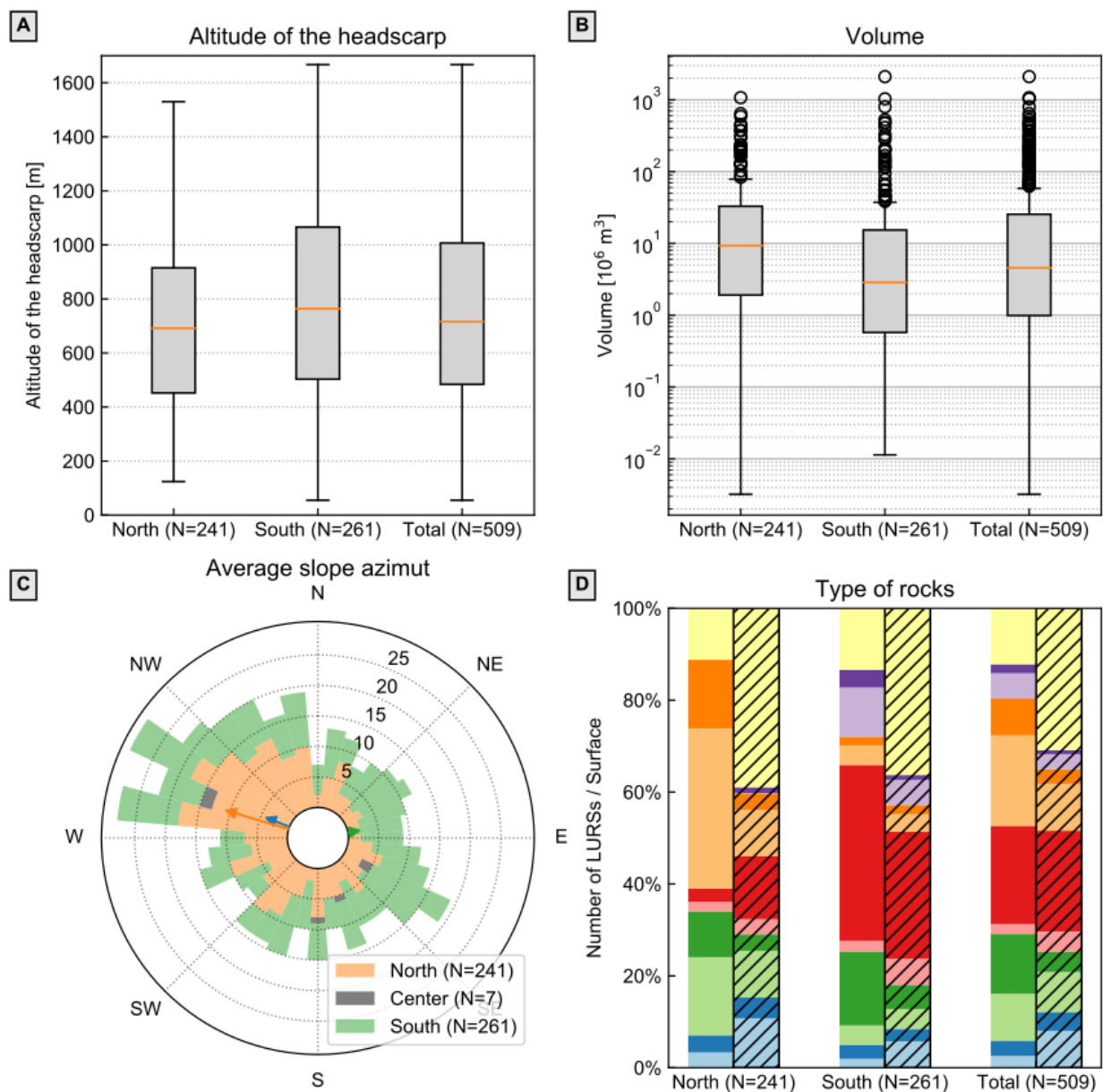
242 p-value, to test for the hypothesis that the two variables do not show a statistical correlation. Although
243 the p-value, which is two-sided, differs from the one obtained using the Chi-squared method, they can
244 be interpreted similarly. This test is applied without filtering or reclassification since it is not influenced
245 by the number of values in a class.

246 **3. RESULTS**

247 **3.1. Distribution of LURs**

248 LURs are spatially concentrated in southern Norway (261) and north of the Polar Circle (241; fig. 1). At a
249 country scale, the median maximum altitude of the headscarps is ca. 700 m a.s.l. (fig. 2A), although
250 higher in the south than in the north. The spatial distribution of LURs is associated with geologic and
251 landscape conditions and the Quaternary history. LURs in southern Norway developed mostly in over-
252 deepened valleys and fjords, and those in northern Norway mainly developed in coastal cliffs carved on
253 flat or gentle relief in Finnmark and in over-deepened valleys and fjords in Troms. The median volume of
254 LURs in northern Norway is $9.3 \cdot 10^6 \text{ m}^3$ and $2.9 \cdot 10^6 \text{ m}^3$ in the South (fig. 2B). The mean orientation of
255 LURs is 291° (WNW) with a vector strength of 0.14, indicating a weak preferential orientation (fig. 2C).
256 This is mostly influenced by the LURs in the North (with a preferential orientation of 287° and a vector
257 strength of 0.36), while there is almost no preferential orientation in the South (with a preferential
258 orientation of 80° and a vector strength of 0.06). 82% of LURs have preferentially developed on five
259 lithologic units, as observed in Figure 2D. In the North, most LURs developed on 1) mica-gneisses, mica-
260 schist, metasandstone and amphibolite, while a minor proportion developed on 2) metasandstones and
261 mica-schist. The high proportion of LURs in unit 1 (35%) is not representative of the distribution of
262 lithologies in this region in which this unit is only outcropping in 10% of the surface (fig. 2D). In the
263 South, most LURs developed on 1) dioritic to granitic gneiss, migmatites, while a minor proportion
264 developed on 2) phyllites, mica-schist. Here, the lithologies in which the LURs developed better match

265 the general distribution of outcrops in that region. The lithologies grouped as “Others” are
 266 underrepresented in the LURs distribution in both regions.



267



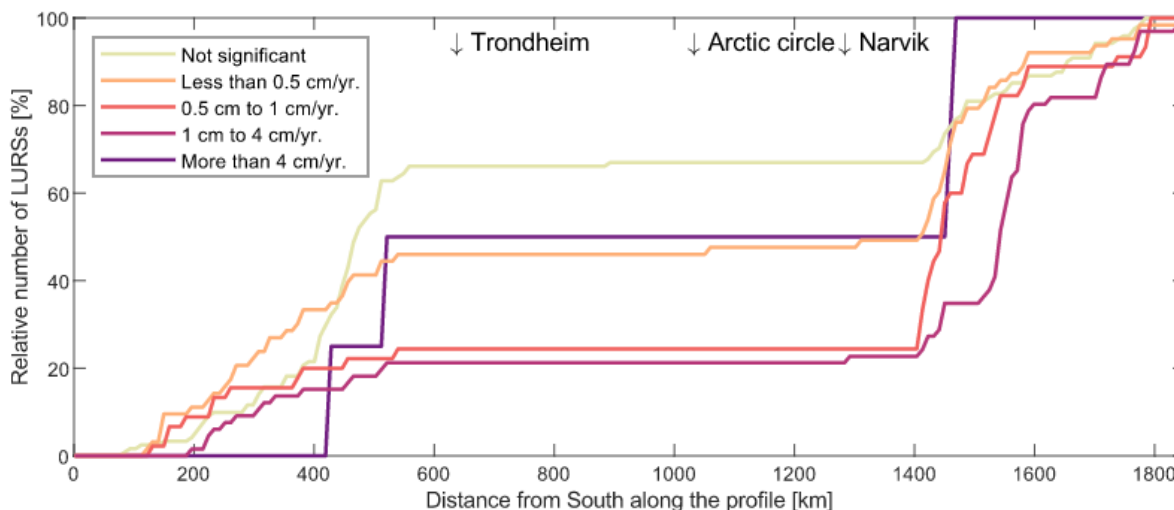
268

269 Figure 2. Characteristics of the LURs. A) Boxplot with altitude of headscarps per region and for the
270 entire country. B) Boxplot with volume of LURs per region and for the entire country. C) Rose diagram
271 with the distribution of slope aspects at which LURs developed. The vectors indicate an eventual
272 preferred orientation, where the vector's length is proportional to its strength. The blue vector is for the
273 whole of Norway; the orange and green are for the North and South respectively. The few LURs from
274 central Norway are shown as an independent class for completeness but are otherwise only included in
275 the total. D) Stack bar showing the distribution of LURs by lithologies, and the proportion of the surface
276 covered by those lithologies in the same regions (with hashed pattern). Lithologies were taken from the
277 1:250 000 harmonized bedrock map database (http://geo.ngu.no/kart/berggrunn_mobil/). Note: Boxes
278 in boxplot represent 25–75% quartiles and whiskers are 1.5 interquartile ranges from the median.
279 Medians are shown as orange lines.

280 **3.2. Current displacement rates of LURs**

281 Displacement rates have been established for ca. 57% of the LURs, and from this, ca. 61% (177) show
282 active displacements. The number of active LURs increases towards the North. Around 60% of the
283 currently inactive LURs are located in southern Norway. The proportion of LURs with displacements
284 slower than 0.5 cm/y is similar throughout Norway. More than 70% of the LURs with displacements
285 ranging 0.5-1 cm/y are located north of the Polar Circle, as are more than 80% of those displacing
286 between 1-4cm/y (fig. 3).

287



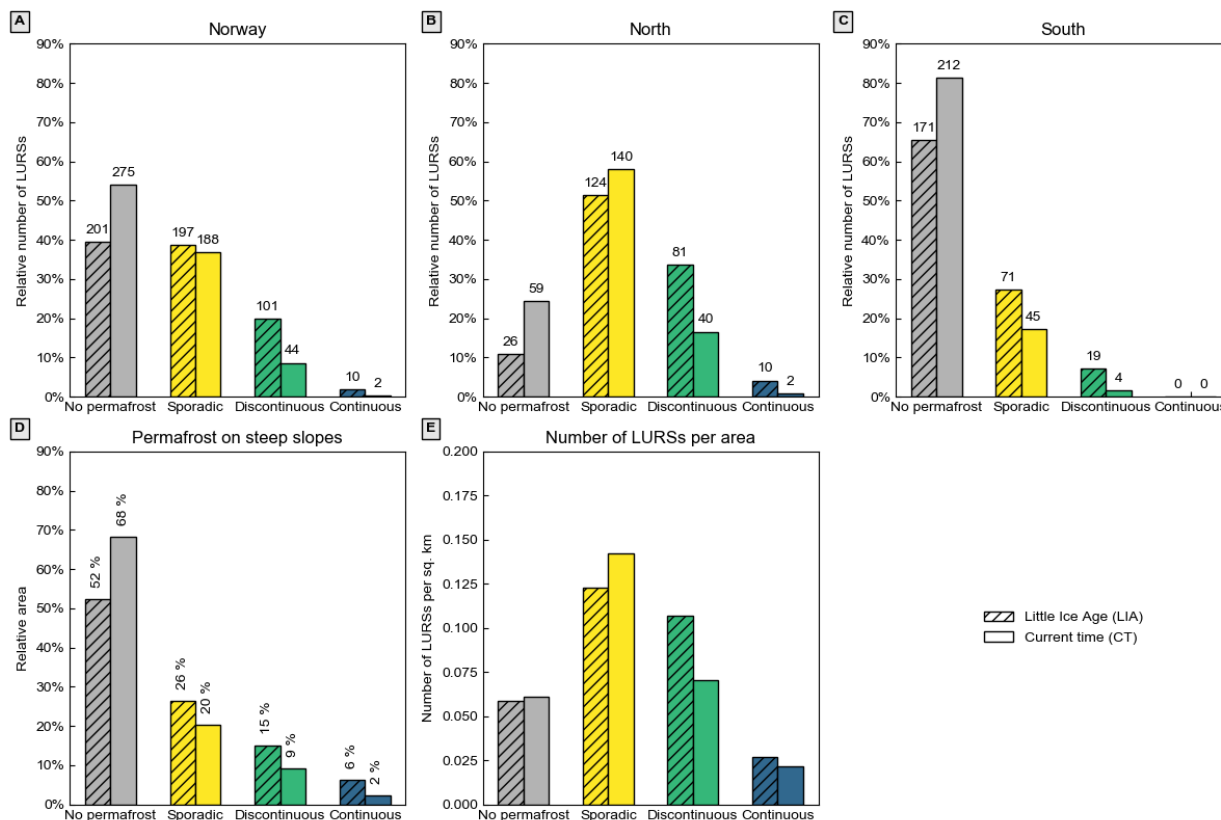
288

289 Figure 3. Cumulative curves of classes of displacement rates from south to north. The location of the
290 LURs and the profile used to build the cumulative curves are displayed on figure 1A.

291 3.3. Past and current permafrost conditions of LURs

292 Steep slopes ($> 40^\circ$ on 10 m resolution DEM), represent around 6000 km² in cartographic area in
293 Norway. Our model shows that approximately 3000 km² of those steep slopes had permafrost
294 (continuous to sporadic) during the LIA. This represents 48 % of the steep slopes' surface area (fig. 4D),
295 meaning that the other 52% had already no permafrost at that time. Our model further shows that 32%
296 of the steep slopes' surface area currently has permafrost, which means that permafrost disappeared in
297 around 16 % of the steep slopes between the LIA and now. In Finnmark (northern Norway), the sporadic
298 permafrost extends down to sea level on coastal cliffs. In the southern extreme of Norway, the current
299 lower limit is at around 700 m a.s.l. At that altitude, only extremely shaded slopes can have permafrost.
300 The lower modelled altitudinal limit of sporadic permafrost during the LIA was at sea level in northern
301 Norway and ca. 270 m a.s.l. in the south.

302 From the modelled permafrost during LIA and the location of the LURs, we observe that during the LIA, a
 303 similar number of LURs existed in permafrost-free and sporadic permafrost areas (fig. 4A). After the
 304 LIA, the reduction in the extent of the permafrost changed the ground conditions of several LURs.
 305 Seventyeight (45 in the South and 33 in the North) of 203 LURs changed from sporadic permafrost to
 306 permafrost-free conditions and 66 (16 in the South and 49 in the North and 1 in the centre) of 103 from
 307 discontinuous to sporadic permafrost. Of the 237 LURs with current permafrost in Norway, ca. 77% are
 308 located north of the Polar Circle. Figure 4 A and D show that the proportion of LURs in the sporadic
 309 permafrost class (around 37% at CT) is higher than the proportion of the surface covered by sporadic
 310 permafrost (around 21% at CT), which gives a higher number of LURs per square kilometer in that class
 311 (fig. 4 E).

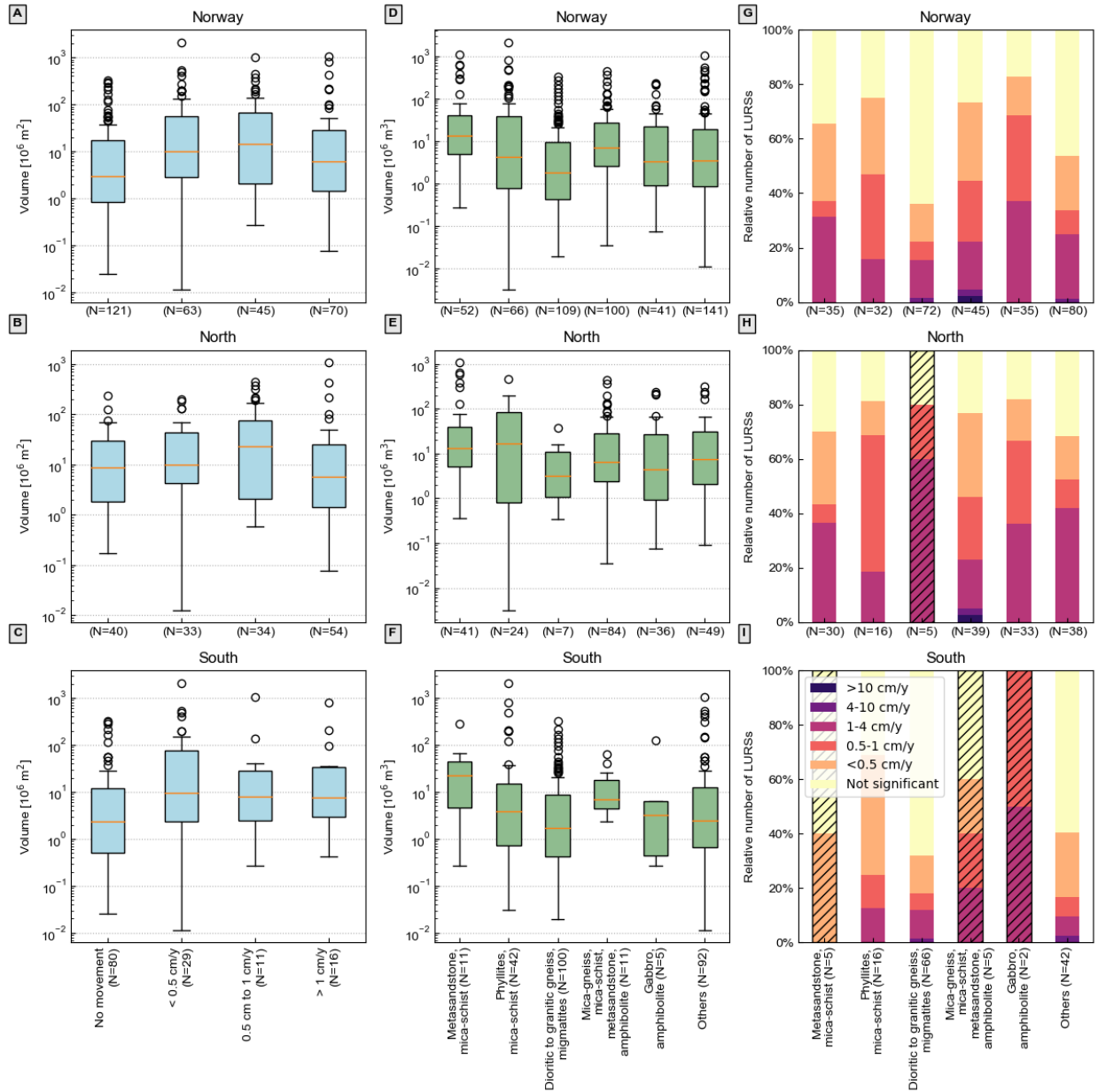


312
 313 Figure 4. Temporal change of type of permafrost present in LURs. A) Histogram showing the proportion
 314 of LURs in each class of permafrost in Norway. B) Histogram showing the proportion of LURs in each

315 class of permafrost in northern Norway. C) Histogram showing the proportion of LURs in each class of
316 permafrost in southern Norway. D) Histogram showing the proportion of steep slopes in each class of
317 permafrost. E) Histogram showing the number of LURs per square kilometre. No permafrost and
318 continuous permafrost are underrepresented in the number of LURs per square kilometre, while
319 sporadic permafrost and discontinuous permafrost (for the latter mostly in the Little Ice Age) are
320 overrepresented.

321 **3.4. Controlling factors of displacement rates - Statistical analyses**

322 The relationships between LURs' volume, lithology, slope, and displacement rates, are presented in fig.
323 5. LURs with smaller volumes seem to have slower displacement rates than the larger ones. However,
324 the pattern is not very clear. Regarding the relation between volume and lithology, we observe that
325 LURs developed on dioritic to granitic gneiss and migmatites are smaller than those developed on other
326 types of rocks. In addition, at the country scale, LURs developed on this type of rock seem to present
327 slower displacements. However, this is because this unit is significantly more represented in the South
328 than in the North, where displacement rates are slower. Indeed, a similar relation is not observed when
329 analysing the North and the South separately.

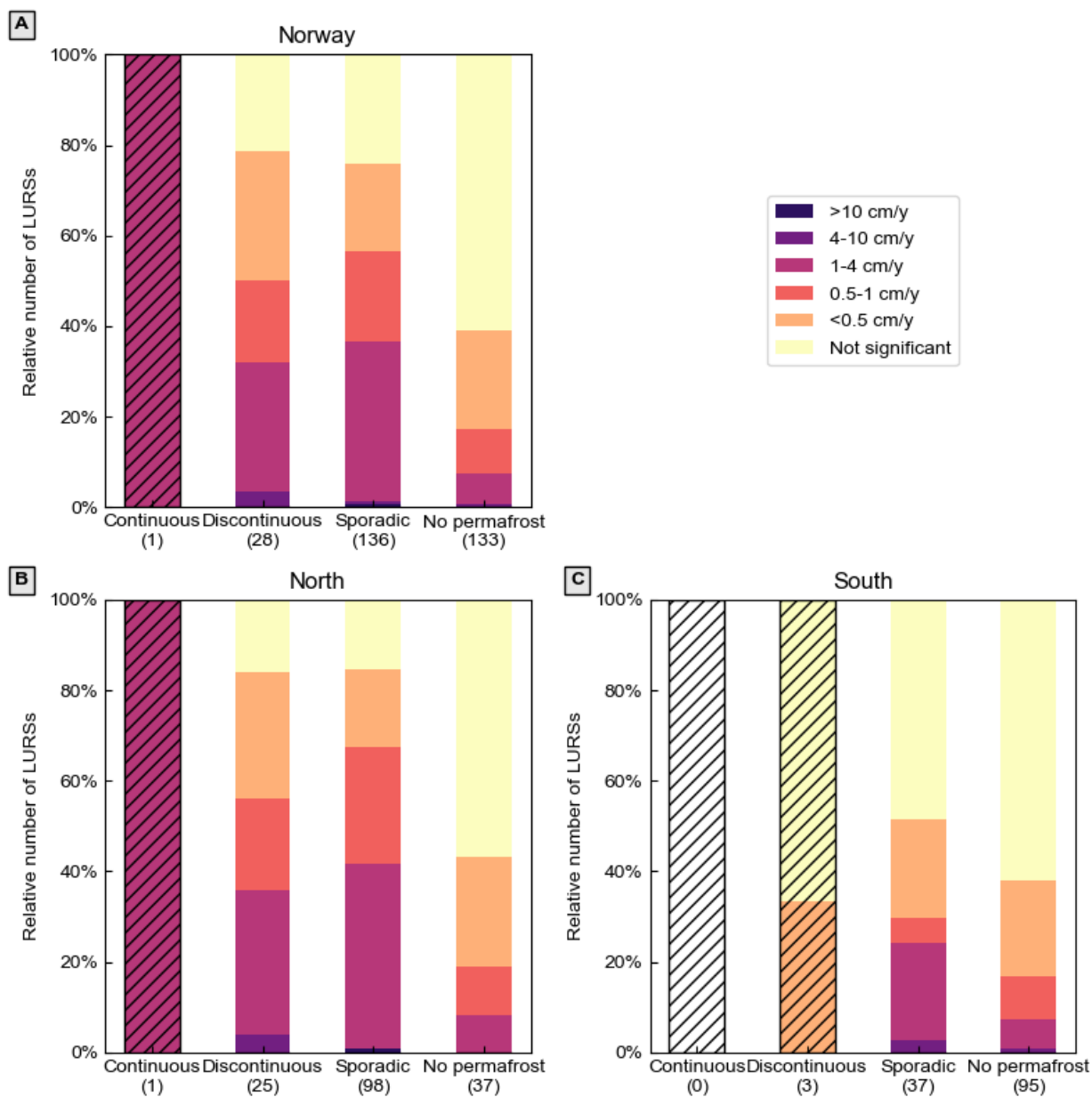


330

331 Figure 5. Boxplots showing the distribution of volumes of LURs by displacement rate class for the whole
 332 country (A), North (B) and South (C) Norway. Box plots showing the distribution of volumes of LURs by
 333 class of lithology for the whole country (D), North (E) and South (F). Stack bars showing the relative
 334 distribution of LURs by lithology and displacement rates classes for the whole country (G), North (H)
 335 and South (I). Note: Boxes in boxplot represent 25–75% quartiles and whiskers are 1.5 interquartile

336 ranges from the median. Medians are shown as orange lines. For (G), (H) and (I) where a class
 337 represents less than 10 LURs, it is overprinted with a hashed pattern.

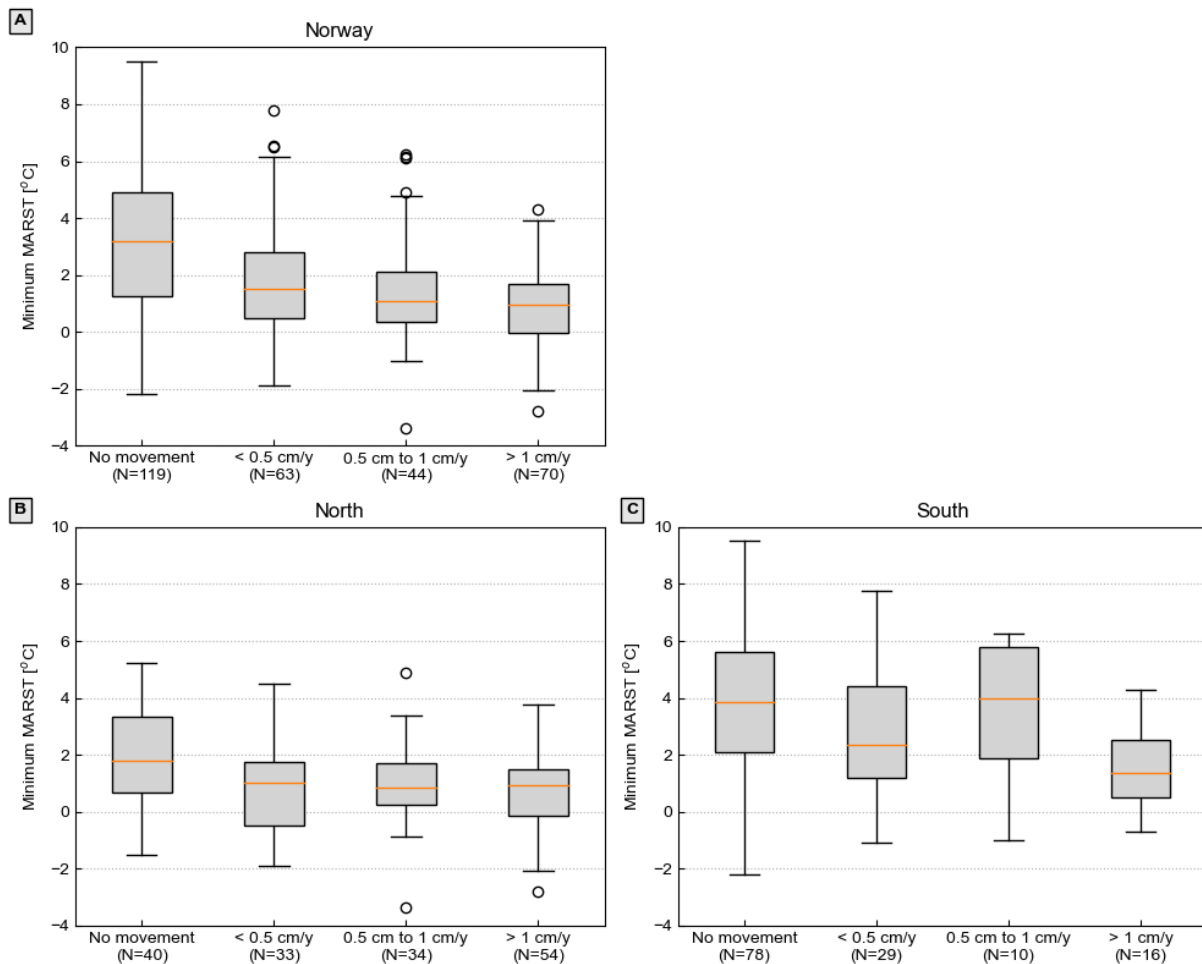
338 Concerning the relation between current permafrost and displacement rates, LURs with no permafrost
 339 show lower displacement rates than those with permafrost in general (fig. 6). Sporadic permafrost hosts
 340 LURs with relatively higher displacement rates than discontinuous permafrost (fig. 6 and fig. S1).



341

342 Figure 6. Stack bar showing the relative distribution of LURs, the type of permafrost and displacement
 343 rate classes for Norway (A), NN (B) and SN (C). Where a class represents less than 10 LURs, it is shown
 344 with higher transparency.

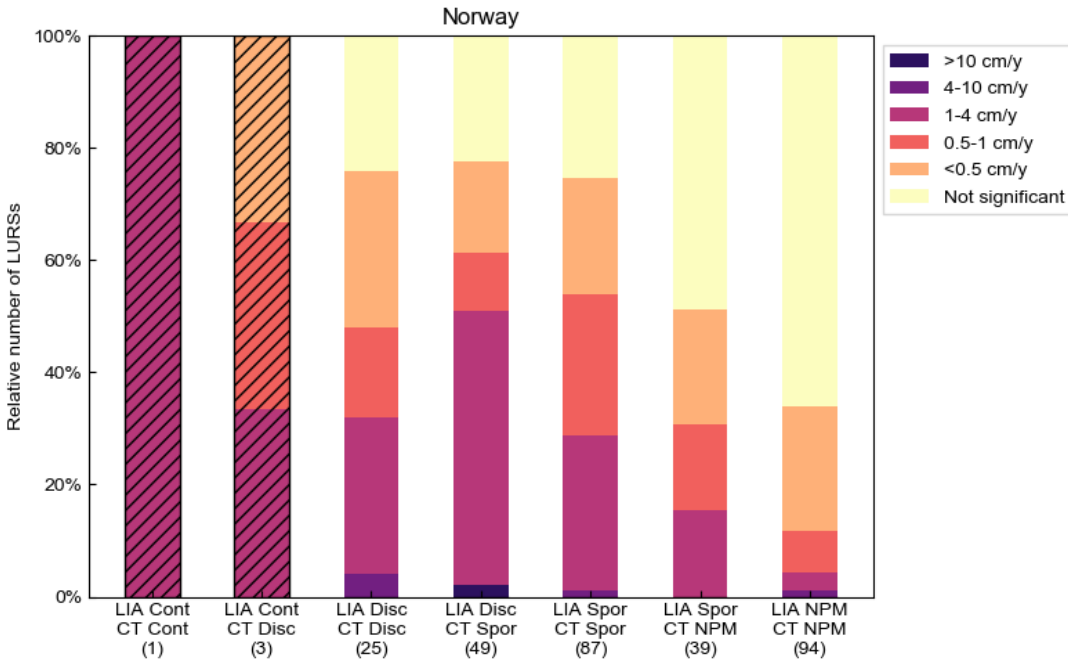
345 The analysis of minimum MARST shows that displacement rates increase with decreasing temperatures
 346 (fig. 7A). This trend is more evident in northern Norway (fig. 7B) and more marked in Troms (fig. S2),
 347 where the range of temperatures is wider. Currently, inactive LURs have an average minimum MARST
 348 over +3°C, while it is close to +1°C for active LURs.



349

350 Figure 7. Boxplots with minimum MARST, and displacement rate classes with amount of LURs present
351 in each class. Note: Boxes represent 25–75% quartiles and whiskers are 1.5 interquartile ranges from the
352 median. Medians are shown as orange lines.

353 The analysis of the distribution of permafrost during the LIA and current time (CT), combined with
354 current displacement rates, shows the link between permafrost conditions and the activity of LURs (fig.
355 8). LURs with permafrost conditions during the LIA are more likely to move than those that did not
356 have permafrost. It is also interesting to observe that the LURs having discontinuous permafrost during
357 the LIA show less movement if they still have discontinuous permafrost than if they have now sporadic
358 permafrost (fig. 8). LURs with no permafrost during the LIA nor in CT are more likely to show no
359 movement or insignificant displacement rates. Globally, ca. 30% of LURs without permafrost conditions
360 during the LIA are currently moving, while ca. 70% of LURs with permafrost conditions during the same
361 period show active displacements. 49% of LURs with permafrost during the LIA but without current
362 permafrost conditions show active displacements, which means that the probability of a LUR being
363 active is 1.6 times higher if the permafrost did not completely thaw between the LIA and CT. These
364 characteristics are visible at the country scale and in the North and South separately (fig. 8 and fig. S3).
365 Of the 25 LURs in the South, where permafrost thawed completely after the LIA, 12 of them do not
366 show current displacement. Of the 18 LURs in the North with displacement information where
367 permafrost thawed completely after the LIA, 10 do not show current displacement.



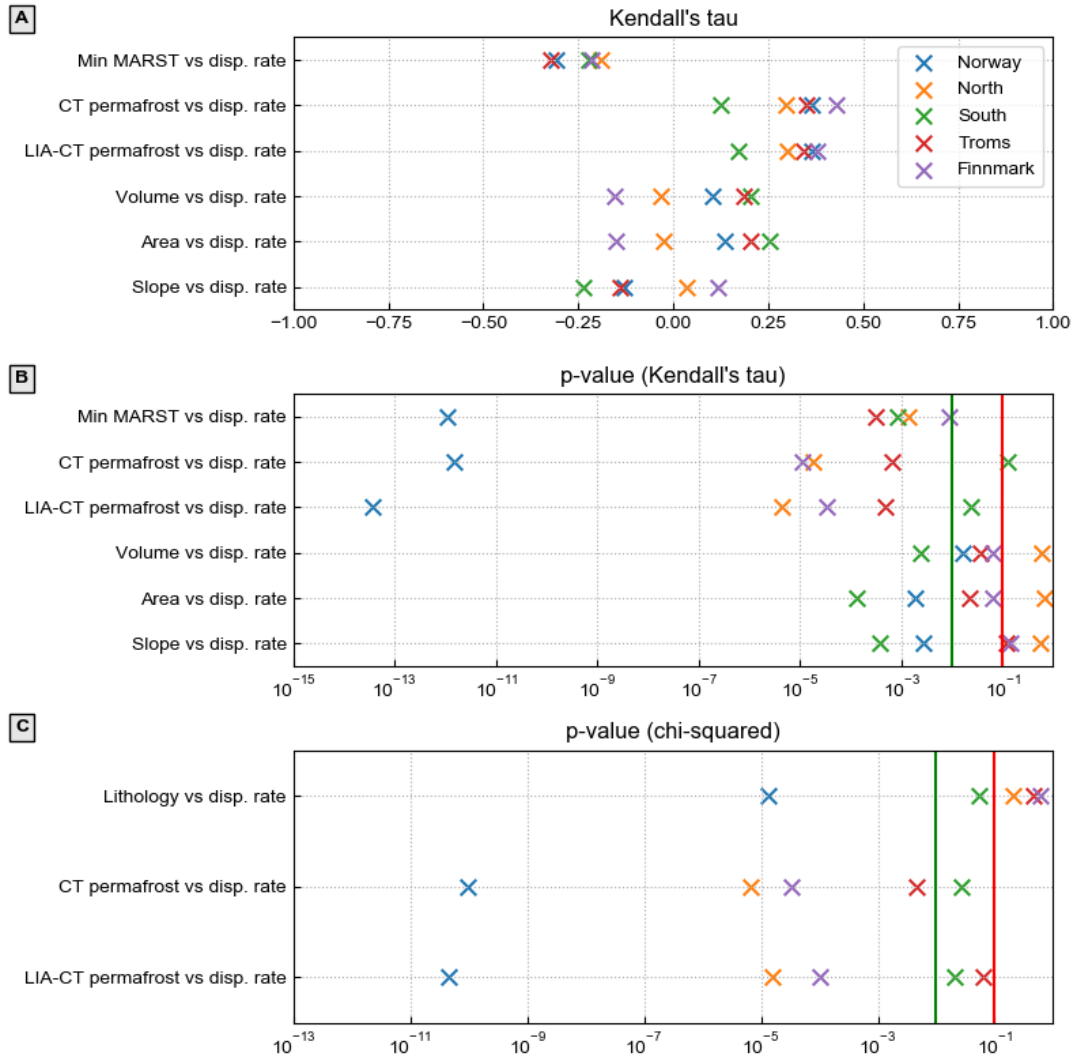
368

369 Figure 8. Stack bar showing the distribution of LURSSs by type of permafrost and during the LIA and
 370 current times (CT), and classified by current displacement rates. Where a class represents less than 10
 371 LURSSs, it is overprinted with a hashed pattern. Classes are ordered first by CT permafrost type, then by
 372 LIA.

373 In the results of the statistical tests (fig. 9), from the values of Kendall's τ , we can observe that the
 374 current type of permafrost is positively associated with the displacement rates, although the association
 375 is moderate. The association is relatively stable for all geographic areas. It is slightly lower in the South,
 376 where permafrost is less widespread (0.16), and has values of 0.31-0.43 for the other regions. The
 377 results are statistically significant with p-values below 0.01, except for the South where the p-value is
 378 partly significant (0.05). The association is also positive for the combination of permafrost during the LIA
 379 and CT (0.21-0.39), with all p-values below 0.01. The association is negative for the minimum MARST
 380 and the displacement rates, meaning lower temperatures correspond with faster displacements. The
 381 association is moderate (-0.18 to -0.33), but statistically significant for all regions. On the other hand, the
 382 trend is not clear for the association of the volume and the displacement, since τ takes both positive and

383 negative values, and since the associated p-value is significant in only one region (South), partly
384 significant in three other regions (Norway, Troms and Finnmark) and not significant in the last region
385 (North). In the South, the association is the largest (0.26), while the p-value is the lowest, which
386 indicates a positive association between the volume and the displacement rates in this area. This is
387 probably related to the large number of smaller LURs developed in dioritic to granitic gneiss and
388 migmatites that tend to have not-significant or no displacements. A relatively similar observation can be
389 done for the association between the slope and the displacement rates. At the country scale, the
390 association is negative (-0.15) and statistically significant, meaning LURs on steeper slopes tend to
391 present less displacement. Similar observations can be made in the South and in Troms, but are only
392 partly statistically significant. No association is observed when looking at the North, and a positive, but
393 statistically not significant association is observed in Finnmark.

394 The p-values obtained with the Chi-squared method (fig. 9) in northern Norway do not show a
395 correlation between lithology and displacement rates. In the South, there is a partial correlation
396 between these parameters. On the other hand, the current permafrost and the displacement rates, as
397 well as the combination of permafrost during the LIA and CT in relation to displacement rates, show a
398 statistical significance for all the regions, except for the correlation of displacement rates and current
399 permafrost in the South, where the p-value is only partly significant.



400

401 Figure 9. Results of the statistical tests for different combinations of variables. A) Kendall's τ indicates
 402 the association of two variables. A value of 1 indicates a perfect monotonically increasing association, a
 403 value of -1 a perfect monotonically decreasing association, and a value of 0 indicates no association.
 404 Both p-values (B and C) indicate the statistical significance of the tests, which are considered statistically
 405 significant below the green line, partly significant between the green and the red lines and not
 406 significant above the red line. Note that permafrost is positively associated with the velocity and the
 407 association is statistically significant. On the other hand, volume, area, slope, or rock type are less clearly
 408 related to the velocity.

409 4. DISCUSSION AND CONCLUSIONS

410 4.1. Uncertainties and limitations

411 Two major uncertainties and limitations arise from this study: (1) the statistical evaluation and (2) the
412 co-existence of permafrost and large unstable rock-slopes.

413 Concerning (1), the Chi-squared and Kendall's τ tests do not differentiate cause-effect from
414 autocorrelation. In our case, we limit the risk of autocorrelation by applying the tests at country-scale, to
415 the North and the South separately and by dividing the North in two. Indeed, since permafrost is mostly
416 present in the North, a correlation with the type of rocks is expected to be seen simply because
417 lithologies are different in the South and the North, while this is less likely inside both regions
418 independently. In addition, we look at different parameters that could explain the difference in
419 displacements, such as size, slope angle, and lithology. Another effect that we do not consider is that
420 Kendall's τ tests test for monotonically increasing or decreasing function. But we see that the relation
421 between permafrost and displacement rates is not monotonical since lower displacement rates are
422 observed and expected where permafrost is either absent or continuous, and higher displacement rates
423 are expected for thawing permafrost (mostly sporadic). However, the low number of LURs in
424 continuous permafrost implies that we are mainly looking at the discontinuous, sporadic and no
425 permafrost classes.

426 Concerning (2), the permafrost conditions are based on a temperature map derived statistically and for
427 steady-state conditions. Other processes that are not accounted for in the statistical approach may
428 impact permafrost conditions, such as topographical and transient effects (Noetzli et al., 2007; Noetzli
429 and Gruber, 2009; Myhra et al., 2017). The topographical effects are related to the variable energy
430 balance at the ground surface that is strongly controlled by direct solar radiation, which depends on sun-
431 exposure and latitude. In Norway, the control of the solar radiation on ground surface temperatures is

432 less than in the European Alps (Hipp et al., 2014; Magnin et al., 2019) and induces temperature
433 difference in the order of 2 to 4°C between north-exposed and south-exposed faces (this decreases with
434 latitude). These differences affect the temperature fields at depth and permafrost that is not expected
435 in a south face when considering statistically-derived surface temperature may exist due to the
436 proximity of a colder north face. This is particularly the case for alpine topography with sharp peaks and
437 spurs. Transient effects that result from the past climatic conditions add to this topographical control.
438 Here again, permafrost may persist at depth even if the predicted permafrost conditions indicate a low
439 probability of its occurrence because of the transient effect of past colder climate. The permafrost map
440 representing current permafrost conditions typically represents conditions for a 30-year period, partially
441 accounting for the recent atmospheric warming (1981-2010). The effect of past and colder decades may
442 persist at depth. In this respect, basing the permafrost classes on permafrost probability limits the risk of
443 misinterpreting the results due to a lack of consideration for past climate because the map users are
444 made aware that a low probability (e.g. probability falling under the sporadic permafrost class) doesn't
445 necessarily mean the absence of permafrost. Other parameters that may favour the existence of
446 permafrost even under low probability are the snow cover and bedrock fractures. Previous
447 investigations show that permafrost might exist below positive surface temperature up to about 3°C
448 depending on sun-exposure (Hasler et al., 2011). For example, the Jettan unstable rock-slope in
449 northern Norway, with ice in deep fractures (Blikra and Christiansen, 2014).

450 **4.2. Permafrost and current displacement rates**

451 In Norway, geologic, landscape, and climate conditions control the development of LURs, their extent
452 and kinematics (Böhme et al., 2013; Booth et al., 2015; Vick et al., 2020). The destabilisation of rock-
453 slopes mainly occurred soon after the Younger Dryas deglaciation, as shown by cosmogenic nuclide
454 dating of sliding surfaces and morphologic assessments (Hermanns et al., 2017; Hilger et al., 2018; Hilger
455 et al., 2021). Differences in precipitation can not explain differences in displacement rates at country

456 scale. While the mean annual precipitation is higher in the southwest coast (Lussana et al., 2018), the
457 higher displacement rates of LURs are measured in the North. The fact that the lithologies in which
458 most LURs developed better match the areal distribution of the lithologies in the South than in the
459 North is primarily due to suitable relief conditions and does not mean LURs have a higher tendency to
460 develop on a specific lithology. Instead, the high relief areas occupy a larger extension in the South than
461 in the North. Similarly, the lithological units classified as “others” are always underrepresented when
462 considering the LURs’ lithology distribution simply because they are widespread in regions with low
463 relief, where no LURs developed and have therefore not been differentiated in this analysis. Regarding
464 the activity of the LURs, a recent study of nine LURs in northern Norway showed their complex nature
465 and pointed out a link between displacements and structural conditions (Vick et al., 2020). In southern
466 Norway, actively displacing LURs are mostly seen on phyllites and mica-schist. In four of those LURs,
467 the poor rock-mass quality was previously proposed as a key control of the active deformation (Böhme
468 et al., 2013; Penna et al., 2017). However, our results show that the correlation between lithologies and
469 displacement rates is only partially significant in the South and not significant in the North. While
470 geologic conditions alone cannot explain the northward increase of displacement rates or even
471 differences in displacement rates in northern Norway, ground temperature variations can. Our results
472 show that permafrost and changes in permafrost co-vary with observed displacement rates, with faster
473 displacement measured in LURs with a MARST closer to 0°C suggesting permafrost at depth. This is
474 caused by the cryostatic and hydrostatic changes induced by the warming of permafrost. The factor of
475 safety of ice-filled fractured rocks decreases when ground temperatures get closer to the ice’s melting
476 point (Davies et al., 2001); it is equal to 1 or more when ice has fully melted or when temperatures are
477 below the melting point. The shear stress decreases when ice-filled joints warm to temperatures close
478 to 0°C (Mamot et al., 2021). In addition, the melting of ice increases the water circulation in jointed
479 rocks, enhancing the hydrostatic pressure of the frozen fractured rocks (Murton et al., 2016).

480 **4.3. Permafrost decline and the hazard paradigm**

481 Since the deglaciation of the Fennoscandian Ice Sheet, the permafrost in Norway has undergone drastic
482 variations (Lilleøren et al., 2012). Fluctuations in the extent of permafrost have an impact on the
483 strength of rock-slopes. Recent works discuss how the aggradation and degradation of permafrost
484 undermine their stability (e.g. Voigtländer et al., 2018; Dräbing and Krautblatter, 2019). Our results
485 show that LURs with discontinuous permafrost during the LIA are more likely to move if they currently
486 have sporadic permafrost than if they currently have discontinuous permafrost. In addition, LURs with
487 permafrost remaining since the LIA are more likely to move than those with permafrost during the LIA
488 that are currently permafrost-free. This has two main implications; firstly, permafrost degradation can
489 increase displacement rates. This is consistent with the outcomes of recent studies on three LURs of
490 northern Norway, located on sporadic or discontinuous permafrost, showing that paleo-slip rates were
491 half of the currently measured ones (Böhme et al., 2019; Hilger et al., 2021). Secondly, the complete
492 thaw of permafrost can lead to a decrease in the displacement rates, and LURs can decelerate until
493 arrest. Both in the North and in the South, half of the LURs whose permafrost thawed completely after
494 the LIA have insignificant displacement rates or no movement. Therefore, the paradigm of permafrost
495 degradation directly increasing the frequency of failures only partially addresses the effect of ground ice
496 melt associated with the thawing of permafrost. This is because active displacements are often seen as
497 the prelude to failure, and forecasts assume constant external forcing factors. But external factors
498 change with time (Carlá et al., 2017). The formation of a sliding surface requires the nucleation of cracks
499 under appropriate environmental and geologic conditions. As environmental conditions change with
500 time, the development of a sliding surface can be accelerated, deaccelerated, interrupted or
501 reactivated. The complete thaw of permafrost removes the hydrostatic pressure and cryostatic pressure
502 from the rock, leaving the shear force induced by gravity and pre-existing stresses as the main drivers of
503 deformation (Krautblatter et al., 2013). Therefore, if during the period of permafrost and permafrost

504 degradation the accumulated deformation was not enough to drive a slope to failure or to lead to the
505 full development of a sliding surface, a LURS can decelerate and halt (dormant state) once permafrost
506 has completely decayed. However, changes in environmental conditions can drive dormant LURs to
507 reactivate. In summary, while permafrost warming at temperatures closer to 0°C can increase the
508 displacement rates of LURs, thereby increasing the hazard level, the complete thaw of the permafrost
509 can lead to a decrease in their displacements, thereby decreasing the hazard level. However, neither
510 increase nor decrease of displacement rates assures or excludes the possibility of a LURS failing
511 catastrophically.

512 **DATA AVAILABILITY**

513 MARST data for current permafrost analysed during this study are included in Magnin et al. (2019;
514 <https://doi.org/10.5194/esurf-7-1019-2019>) and its supplementary information files
515 (<https://doi.org/10.5194/esurf-7-1019-2019-supplement.>).

516 The modelled permafrost map for the Little Ice Age is available from the corresponding author under
517 request.

518 InSAR data is freely available at <https://insar.ngu.no>

519 LURs data is freely available at https://geo.ngu.no/kart/ustabilefjellparti_mobil/

520 Bedrock map available at: https://geo.ngu.no/kart/berggrunn_mobil/

521 **REFERENCES**

522 Agresti, A., 2010. Analysis of Ordinal Categorical Data (Second ed.). Wiley Series in Probability and
523 Statistics. New York: John Wiley & Sons. <http://dx.doi.org/10.1002/9780470594001>

524 Allen, S. K. Gruber, S., Owens, I. F., 2009. Exploring steep bedrock permafrost and its relationship with
525 recent slope failures in the Southern Alps of New Zealand. *Permafr. Periglac. Process.* 20 (4), 345–356.
526 <https://doi.org/10.1002/ppp.658>.

527 Bertolo, D. A., 2017. Decision support system (DSS) for critical landslides and rockfalls and its application
528 to some cases in the Western Italian Alps. *Nat. Hazards Earth Syst. Sci. Discuss.*:1–31.
529 <https://doi.org/10.5194/nhess-2017-396>

530 Biskaborn, B. K. et al., 2019. Permafrost is warming at a global scale. *Nat. Commun.* 10, 264.
531 <https://doi.org/10.1038/s41467-018-08240-4>

532 Blikra, L.-H. Longva, O. Braathen, A. Anda, E. Dehls, J., Stalsberg, K., 2006. Rock slope failures in
533 Norwegian fjord areas: examples, spatial distribution and temporal pattern. In: Evans S.G., Mugnozza
534 G.S., Strom A., Hermanns R.L. (eds) *Landslides from Massive Rock Slope Failure*. NATO Science Series, vol
535 49. Springer, Dordrecht.

536 Blikra, L. H., Christiansen, H. H., 2014. A field-based model of permafrost-controlled rockslide
537 deformation in northern Norway. *Geomorphology.* 208, 34–49.
538 <https://doi.org/10.1016/j.geomorph.2013.11.014>

539 Böhme, M., Hermanns, R. L., Oppikofer, T., Fischer, L., Bunkholt, H. S., Eiken, T., Pedrazzini, A., Derron,
540 M.-H., Jaboyedoff, M., Blikra, L. H., 2013. Analysing complex rock slope deformation at Stampa, western
541 Norway, by integrating geomorphology, kinematics and numerical modeling. *Eng. Geol.* 154, 116-130.

542 Böhme, M., Hermanns, R.L., Gosse, J., Hilger, P., Eiken, T., Lauknes, T.R., Dehls, J.F., 2019. Comparison of
543 monitoring data with paleo-slip rates: Cosmogenic nuclide dating detects acceleration of a rockslide.
544 *Geology.* 47(4), 339–342. <https://doi.org/10.1130/G45684.1>

545 Booth, A. M. Dehls, J. Eiken, T. Fischer, L. Hermanns, R. L., Oppikofer, T., 2015. Integrating diverse
546 geologic and geodetic observations to determine failure mechanisms and deformation rates across a
547 large bedrock landslide complex: the Osmundneset landslide, Sogn og Fjordane, Norway. *Landslides*. 12
548 (4), 745-756. <https://doi.org/10.1007/s10346-014-0504-y>

549 Borradaile, G., 2003. *Statistics of Earth Science Data*. Springer-Verlag. ISBN 978-3-662-05223-5

550 Carlá, T., Intrieri, E., Di Traglia, F., Nolesini, T., Gigli, G., Casagli, N., 2017. Guidelines on the use of inverse
551 velocity method as a tool for setting alarm thresholds and forecasting landslides and structure collapses.
552 *Landslides*. 14, 517–534. <https://doi.org/10.1007/s10346-016-0731-5>

553 Davies, M. C. Hamza, O., Harris, C., 2001. The effect of rise in mean annual temperature on the stability
554 of rock slopes containing ice-filled discontinuities. *Permafr. Periglac. Process*. 12, 137–144.
555 <https://doi.org/10.1002/ppp.378>

556 Dehls, J. F. Larsen, Y. Marinkovic, P. Lauknes, T. R. Stødle, D., Moldestad, D. A., 2019. INSAR.No: A
557 National Insar Deformation Mapping/Monitoring Service In Norway -- From Concept To Operations.
558 IGARSS 2019 - 2019 IEEE International Geoscience and Remote Sensing Symposium, p. 5461-5464, doi:
559 10.1109/IGARSS.2019.8898614.

560 Dräbing, D., Krautblatter, M., 2019. The Efficacy of Frost Weathering Processes in Alpine Rockwalls.
561 *Geophys. Res. Lett.* 46 (12), 6516-6524. <https://doi.org/10.1029/2019GL081981>

562 Etzelmüller, B., Patton, H., Schomacker, A., Czekirda, J., Girod, L., Hubbard, A., Lilleøren, K. S.,
563 Westermann, S., 2020. Icelandic permafrost dynamics since the Last Glacial Maximum—model results
564 and geomorphological implications. *Quat. Sci. Rev.* 233, 106236.
565 <https://doi.org/10.1016/j.quascirev.2020.106236>

566 Ferretti, A. Prati, C., Rocca, F., 2000. Nonlinear subsidence rate estimation using permanent scatterers in
567 differential SAR interferometry. *IEEE Trans. Geosci. Remote Sens.* 38(5), 2202–2212.

568 Ferretti, A. Prati, C., Rocca, F., 2001. Permanent scatterers in SAR interferometry. *IEEE Trans. Geosci.*
569 *Remote Sens.* 39(1), 8–20.

570 Fischer, L. Amann, F. Moore, J. R., Huggel, C., 2010. Assessment of periglacial slope stability for the 1988
571 Tschierwa rock avalanche (Piz Morteratsch, Switzerland). *Eng. Geol.* 116, 32–43.
572 <https://doi.org/10.1016/j.enggeo.2010.07.005>

573 Gislås, K., Etzelmüller, B., Lussana, C., Hjort, J., Sannel, B., Isaksen, K., Westermann, S., Kuhry, P.,
574 Christiansen, H. H., Frampton, A., Åkermann, J., 2016a. Permafrost map for Norway, Sweden and
575 Finland. *Permafrost Periglacial Process.* 28 (2), 359-378.

576 Gislås, K., Westermann, S., Vikhamar Schuler, T., Melvold, K., Etzelmüller, B., 2016b. Small-scale variation
577 of snow in a regional permafrost model. *The Cryosphere.* 10, 1201–1215.
578 <https://doi.org/10.1002/ppp.1922>

579 Gruber, S. Hoelzle, M., Haeberli, W., 2004. Permafrost thaw and destabilisation of Alpine rock walls in
580 the hot summer of 2003. *Geophys. Res. Lett.* 31, L13504. <https://doi.org/10.1029/2004GL020051>

581 Haeberli, W. Wegmann, M., Vonder Mühll, D., 1997. Slope stability problems related to glacier shrinkage
582 and permafrost degradation in the Alps. *Eco. Geol. Helv.* 90, 407–414.

583 Hasler, A. Gruber, S., Haeberli, W., 2011. Temperature variability and offset in steep alpine rock and ice
584 faces. *The Cryosphere.* 5, 977–988. <https://doi.org/10.5194/tc-5-977-2011>.

585 Hermanns, R., Oppikofer, T., Anda, E., Blikra, L., Böhme, M., Bunkholt, H., Crosta, G., Dahle, H., Devoli,
586 G., Fischer, L., 2012. Recommended hazard and risk classification system for large unstable rock slopes
587 in Norway: NGU rapport 2012.029, p. 53.

588 Hermanns, R., Blikra, L., Anda, E., Saintot, A., Dahle, H., Oppikofer, T., Fischer, L., Bunkholt, H., Böhme,
589 M., Dehls, J., Lauknes, T., Redfield, T., Osmundsen, P., Eiken, T., 2013. Systematic Mapping of Large
590 Unstable Rock Slopes in Norway, in Margottini, C., Canuti, P., and Sassa, K., eds., *Landslide Science and*
591 *Practice*, Springer Berlin Heidelberg, 29–34.

592 Hermanns, R.L., Schleier, M., Böhme, M., Blikra, L. H., Gosse, J., Ivy-Ochs, S., Hilger, P., 2017. Rock-
593 Avalanche Activity in W and S Norway Peaks After the Retreat of the Scandinavian Ice Sheet, in
594 *Proceedings Workshop on World Landslide Forum 2017*, Springer, 331-338.

595 Hilger, P. Hermanns, R. L. Gosse, J. C. Jacobs, B. Etzelmüller, B., Krautblatter, M., 2018. Multiple rock-
596 slope failures from Mannen in Romsdal Valley, western Norway, revealed from Quaternary geological
597 mapping and ¹⁰Be exposure dating. *The Holocene*. 28(12), 1841-1854.
598 <https://doi.org/10.1177/0959683618798165>

599 Hilger, P. Hermanns, R. Czekirda, J. Myhra, K. S. Gosse, J., Etzelmüller, B., 2021. Permafrost as a first
600 order control on long-term rock-slope deformation in the (Sub-)Arctic. *Quat. Sci. Rev.* 251(1), 106718.
601 <https://doi.org/10.1016/j.quascirev.2020.106718>

602 Hipp, T. Etzelmüller, B., Westermann, S., 2014. Permafrost in Alpine Rock Faces from Jotunheimen and
603 Hurrungane, Southern Norway. *Permafr. Periglac. Process.* 25, 1–13. <https://doi.org/10.1002/ppp.1799>

604 Hjort, J., Karjalainen, O., Aalto, J., Westermann, S., Romanovsky, V. E., Nelson, F. E., Etzelmüller, B.,
605 Luoto, M., 2018. Degrading permafrost puts Arctic infrastructure at risk by mid-century. *Nat. Commun.* 9
606 (1), 5147. <https://doi.org/10.1038/s41467-018-07557-4>

607 Huggel, C. Clague, J. J., Korup, O., 2012. Is climate change responsible for changing landslide activity in
608 high mountains? *Earth Surf. Process. Landf.* 37, 77–91. <https://doi.org/10.1002/esp.2223>

609 Jaboyedoff, M. Carrea, D. Derron, M.-H. Oppikofer, T. Penna, I. M., Rudaz, B., 2020. A review of methods
610 used to estimate initial landslide failure surface depths and volumes. *Eng. Geol.* 267, 105478.
611 <https://doi.org/10.1016/j.enggeo.2020.105478>

612 Kondratjeva, K. A, Khruzky, S. F., Romanovsky, N. N., 1993. Changes in the extent of permafrost during
613 the late quaternary period in the territory of the former Soviet Union. *Permafrost Periglacial Process.* 4 (2),
614 113–119.

615 Krautblatter, M. Funk, D., Günzel, F. K., 2013. Why permafrost rocks become unstable: a rock–ice-
616 mechanical model in time and space. *Earth Surf. Process. and Landf.* 38, 876–887.
617 <https://doi.org/10.1002/esp.3374>

618 Kristensen, L., Czekirda, J., Penna, I., Etzelmüller, B., Nicolet, P., Pullarello, J.S., Blikra, L.-H., Skrede, I.,
619 Oldani, S., Abellán, A., 2021. Movements, failure and climatic control of the Veslemannen rockslide,
620 Western Norway. *Landslides.* 18, 1963–1980. <https://doi.org/10.1007/s10346-020-01609-x>

621 Lewkowicz, A. G., Harris, C., 2005. Frequency and magnitude of active-layer detachment failures in
622 discontinuous and continuous permafrost, northern Canada. *Permafrost Periglacial Process.* 16, 115–130.
623 <https://doi.org/10.1002/ppp.522>

624 Lewkowicz, A., Way, R. G., 2019. Extremes of summer climate trigger thousands of thermokarst
625 landslides in a High Arctic environment. *Nat. Commun.* 10, 1329. [https://doi.org/10.1038/s41467-019-](https://doi.org/10.1038/s41467-019-09314-7)
626 [09314-7](https://doi.org/10.1038/s41467-019-09314-7)

627 Liljedahl, A. K. et al., 2016. Pan-Arctic ice-wedge degradation in warming permafrost and its influence on
628 tundra hydrology. *Nat. Geos.* 9, 312–318. <https://doi.org/10.1038/ngeo2674>

629 Lilleøren, K. Etzelmüller, B. Schuler, V.T. Gislås, K., Humlum, O., 2012. The relative age of mountain
630 permafrost — estimation of Holocene permafrost limits in Norway. *Glob. and Planet. Change.* 92-93,
631 209–223. <https://doi.org/10.1016/j.gloplacha.2012.05.016>

632 Lussana, C. Saloranta, T. Skaugen, T. Magnusson, J. Tveito, O.E., Andersen, J., 2018. seNorge2 daily
633 precipitation, and observational gridded dataset over Norway from 1957 to the present day. *Earth Syst.*
634 *Sci. Data.* 10, 235–249.

635 Magnin, F. Etzelmüller, B. Westermann, S. Isaksen, K. Hilger, P., Hermanns, R. L., 2019. Permafrost
636 distribution in steep rock slopes in Norway: measurements, statistical modelling and implications for
637 geomorphological processes. *Earth Surf. Dynam.* 7, 1019–1040. [https://doi.org/10.5194/esurf-7-1019-](https://doi.org/10.5194/esurf-7-1019-2019)
638 2019

639 Mamot, P. Weber, S. Schröder, T., Krautblatter, M., 2018. A temperature- and stress-controlled failure
640 criterion for ice-filled permafrost rock joints. *The Cryosphere.* 12, 3333–3353.
641 <https://doi.org/10.5194/tc-12-3333-2018>

642 Mamot, P. Weber, S. Eppinger, S., Krautblatter, M., 2021. A temperature-dependent mechanical model
643 to assess the stability of degrading permafrost rock slopes. *Earth Surf. Dyn.* 9, 1125–1151.
644 <https://doi.org/10.5194/esurf-9-1125-2021>

645 Massonnet, D., Feigl, K. L., 1998. Radar interferometry and its application to changes in the Earth's
646 surface. *Rev. Geophys.* 36, 441–500. <https://doi.org/10.1029/97RG03139>

647 Murton, J., Kuras, O., Krautblatter, M., Cane, T., Tschofen, D., Uhlemann, S., Schober, S., Watson, P.,
648 2016. Monitoring rock freezing and thawing by novel geoelectrical and acoustic techniques. *J. Geophys.*
649 *Res.* 121, 2309–2332. <https://doi.org/10.1002/2016JF003948>.

650 Myhra, K. S. Westermann, S., Etzelmüller, B., 2017. Modelled Distribution and Temporal Evolution of
651 Permafrost in Steep Rock Walls Along a Latitudinal Transect in Norway by CryoGrid 2D. *Permafr.*
652 *Periglac. Process.* 28, 172-82. <https://doi.org/10.1002/ppp.1884>

653 Noetzli, J. Gruber, S. Kohl, T. Salzmänn, N., Haeberli, W., 2007. Three-dimensional distribution and
654 evolution of permafrost temperatures in idealized high-mountain topography. *J. of Geoph. Research.*
655 112. <https://doi.org/10.1029/2006JF000545>.

656 Noetzli, J., Gruber, S., 2009. Transient thermal effects in Alpine permafrost. *The Cryosphere.* 3, 85–99.
657 <https://doi.org/10.5194/tc-3-85-2009>

658 Obu, J., Westermann, S., Bartsch, A., Berdnikov, N., Christiansen, H.H., Dashtseren, A., Delaloye, R.,
659 Elberling, B., Etzelmüller, B., Kholodov, A., 2019. Northern Hemisphere permafrost map based on TTOP
660 modelling for 2000–2016 at 1 km² scale. *Earth Sci. Rev.* 193, 299–316.
661 <https://doi.org/10.1016/j.earscirev.2019.04.023>

662 Oppikofer, T., Nordahl, B., Bunkholt, H., Nicolaisen, M., Jarna, A., Iversen, S., Hermanns, R. L., Böhme,
663 M., Molina, F. X. Y., 2015. Database and online map service on unstable rock slopes in Norway—From
664 data perpetuation to public information. *Geomorphology.* 249, 69-81.
665 <https://doi.org/10.1016/j.geomorph.2015.08.005>

666 Oppikofer, T. Böhme, M. Nicolet, P. Penna, I., Hermanns, R. L., 2016. Metodikk for konsekvensanalyse av
667 fjellskred. Norges geologiske undersøkelse Available at:
668 http://www.ngu.no/upload/Publikasjoner/Rapporter/2016/2016_047.pdf.

669 Pearson, K., 1900. On the criterion that a given system of deviations from the probable in the case of a
670 correlated system of variables is such that it can be reasonably supposed to have arisen from random
671 sampling. *The London, Edinburgh and Dublin Phil Mag J Sci Ser.* 5 50,157–175.

672 Penna, I. Böhme, M. Hermanns, R. L. Eiken, T., Dehls, J., 2017. Large-Scale Rockslope Deformations in
673 Sogn Og Fjordane County (Norway). In Mikoš, M., Casagli, N., Yin, Y., and Sassa, K. (eds.), *Advancing*
674 *Culture of Living with Landslides*. World Landslide Forum 2017. Springer International Publishing, Cham,
675 601–606.

676 Phillips, M. Wolter, A. Lüthi, R. Amann, F. Kenner, R., Bühler, Y., 2017. Rock slope failure in a recently
677 deglaciated permafrost rock wall at Piz Kesch (Eastern Swiss Alps), February 2014. *Earth Surf. Process.*
678 *and Landf.* 42, p. 426-438. <https://doi.org/10.1002/esp.3992>

679 Ravanel, L., Deline, P., 2011. Climate influence on rockfalls in high-Alpine steep rockwalls: The north side
680 of the Aiguilles de Chamonix (Mont Blanc massif) since the end of the 'Little Ice Age'. *The Holocene*. 21
681 (2), 357–365. <https://doi.org/10.1177/0959683610374887>

682 Ravanel, L. Magnin, F., Deline, P., 2017. Impacts of the 2003 and 2015 summer heatwaves on
683 permafrost-affected rock-walls in the Mont Blanc massif. *Sci. Total Environ.* 609, 132–143.
684 <https://doi.org/10.1016/j.scitotenv.2017.07.055>

685 Shugar, D. et al., 2021. A massive rock and ice avalanche caused the 2021 disaster at Chamoli, Indian
686 Himalaya. *Science*. 373(6552), 300-306. DOI: 10.1126/science.abh4455

687 Svennevig, K., Dahl-Jensen, T., Keiding, M., Merryman Boncori, J.P., Larsen, T.B., Salehi, S., Munck
688 Solgaard, A., Voss, P.H., 2020. Evolution of events before and after the 17 June 2017 rock avalanche at
689 Karrat Fjord, West Greenland – a multidisciplinary approach to detecting and locating unstable rock
690 slopes in a remote Arctic area. *Earth Surf. Dynam.* 8 (4), 1021–1038. [https://doi.org/10.5194/esurf-8-](https://doi.org/10.5194/esurf-8-1021-2020)
691 1021-2020

692 Swindles, G. T. et al., 2015. The long-term fate of permafrost peatlands under rapid climate warming.
693 *Nat. Scientif. Rep.* 5, 17951. <https://doi.org/10.1038/srep17951>

694 Vick, L. M. Böhme, M. Rouyet, L. Bergh, S. G. Corner, G. D., Lauknes, T. R., 2020. Structurally controlled
695 rock slope deformation in northern Norway. *Landslides*. 17, 1745–1776.

696 <https://doi.org/10.1007/s10346-020-01421-7>

697 Voigtländer, A., Leith, K., Krautblatter, M., 2018. Subcritical crack growth and progressive failure in
698 Carrara marble under wet and dry conditions. *J. Geophys. Res. Solid Earth*. 123(5), 3780-3798.

699 <https://doi.org/10.1029/2017JB014956>

700 Wasowski, J., Bovenga, F., 2014. Investigating landslides and unstable slopes with satellite Multi
701 Temporal Interferometry: Current issues and future perspectives. *Eng. Geol.* 174, 103–138.

702 <https://doi.org/10.1016/j.enggeo.2014.03.003>

703 **ACKNOWLEDGEMENTS**

704 The authors acknowledge the Norwegian Water Resources and Energy Directorate for funding most of
705 the research done in the framework of this study. Parts of the study are based on results from the project
706 ‘CryoWALL – Permafrost slopes in Norway’ (243784/CLE) funded by the Research Council of Norway (RCN)
707 at the University of Oslo, Norway.

708 **CONTRIBUTIONS**

709 P,I., Conceptualization, Investigation, Formal Analysis, Writing.

710 M,F., Conceptualization, Methodology, Formal Analysis, Writing.

711 N,P., Methodology, Investigation, Formal Analysis, Graphs, Writing.

712 E,B., Conceptualization, Writing-reviewing.

713 H,R,L., Investigation, Supervision.

714 B,M., Investigation, Writing.

715 K,L., Investigation, Writing.

716 N,F., Investigation, Methodology.

717 B,M., Investigation, Methodology.

718 D,J.F., Investigation, Methodology.

719 All authors have read and approved the final manuscript.

720 **CORRESPONDING AUTHOR**

721 Correspondence to Ivanna Penna (ivana.penna@ngu.no)